Potential consequences of ion beam analysis on objects from our cultural heritage: An appraisal

Alessandro Zucchiatti *, Fernando Agulló-Lopez

Centro de Micro Análisis de Materiales, Universidad Autónoma de Madrid, c/Faraday 3, 28049 Madrid, Spain

A B S T R A C T

The archaeometric application of IBA is possible because in the majority of cases the working conditions are such that no damage and in particular visible damage is produced on the valuable unique samples. Obviously this does not mean that cultural heritage materials do not experience, like all other, the probe-target interaction and effects, but that the interaction is controllable and kept below safe limits. This work has aimed at establishing within which limits the potential damage is negligible or the analysis is viable on the basis of the benefit/cost ratio, making use of the information which is available not only from archaeometry but also from the more "aggressive" materials science applications of ion beams.

© 2012 Elsevier B.V. All rights reserved.

1. Introduction

The application of ion beam analysis (IBA) techniques to the study of our cultural heritage (CH) has been an undeniable success story marked by a continuous growth in terms of numbers of studies, technical developments and novel protocols [1–3]. The number of accelerator laboratories worldwide who have dedicated an IBA beamline to archaeometry has grown considerably since the installation of the AGLAE accelerator inside the Louvre Museum in 1989 [4]. AGLAE is a landmark of the field being the first and only one ever built inside a museum. The reasons of the success are essentially the relative simplicity of the setup of the IBA techniques, in particular PIXE, the possibility of obtaining quite rapidly results that can be exploited to solve a number of recurrent questions, the accessibility of the techniques to scholars, archaeologists, etc., due to the dissemination and coordination actions of the main European laboratories [5–8] and, last but not least, the user's clear perception of the conservation of the integrity of the object during all the analytical steps and the absence of remnant effects (e.g. activation) after the analysis. Besides the direct experience of the users, the physicists and accelerator specialists have always given emphasis to the peculiar non-destructive character of the IBA in almost all their publications. On the other hand, the papers dedicated to the study of the damage induced on the object by the analysis with

an ion beam have been a minor part of the total and most of them have focused on the discussion of visible damage [9–11].

The analysis is one of the uses that can be made of an ion beam impinging on a sample; the other is the radical modification of the physical properties of the materials induced by the ion-material interaction at different levels. This means that, besides archaeometry, we have available a large amount of information concerning the modification of materials that we may exploit to assess the risk of damage (evidently unwanted) in an archaeometric application, depending on the experimental conditions and on the materials concerned. It is therefore possible to make an appraisal of the effects that the ion beam will produce in the sample, evaluate the onset of unwanted effects and define the limits for close to ideal analysis conditions, where the analytical possibilities of the techniques are enhanced while keeping to low and possibly negligible levels the effects of the ion-material interaction. It has to be stressed that by their nature the IBA analyses are best convenient for inorganic materials. This class of materials is possibly the most abundant in what is today our CH due in particular to its ability to resist modifications and alterations during time and even in adverse conservation conditions (e.g. burial). Stones, clays, minerals, glass and glazes, metals are not only much better preserved than wood, paper, textiles, skins but do also stand much better an ion beam analysis. This is why our appraisal concerns mostly inorganic materials.

Quite recently the synchrotron radiation has been established as a complementary and alternative approach to the study of our CH making available a consistent number of hours and quite a

* Corresponding author. Tel.: +34 914972791; fax: +34 914973623.
  E-mail address: alessandro.zucchiatti@uam.es (A. Zucchiatti).

range of sensitive techniques [12]. IBA remains very competitive [13–15] and continues to be the main scientific support to number of studies aimed at establishing provenance, manufacturing techniques, authorship and date of antique artefacts.

2. IBA of cultural heritage

Along the years the beamlines dedicated to the IBA of CH objects have been progressively adjusted to the most common needs of such a kind of analyses and have resulted, at the end, in an almost standard set-up, adopted in many laboratories [16–21]. Samples are analyzed by a combination of techniques; namely PIXE, RBS and PIGE, almost always with an external micro-beam. The examples of ERDA and NRA analyses of our CH are only a few and cannot be considered routine practice even in the laboratories that have developed these techniques with external beams [22,23]. The most used ions are protons and alphas which can be made, tuning their energies, to reach similar penetration ranges into the target. A 12 MeV alpha particle will have a penetration range in a material close to that of a 3 MeV proton. The external micro-beams achieve currents of a few nA and a size from 20 to 150 μm FWHM on the target placed 3–5 mm downstream of a fine (e.g. kapton 7 μm thick) or ultrafine (0.1 μm-thick Si_3N_4) exit membrane that allows to transmit the particle beam from the vacuum pipe of the accelerator to the air where the sample sits. The emitted characteristic X-rays are analyzed, quite conventionally by two X-ray detectors (tipically of the Si(Li) or the SDD type, liquid nitrogen or Peltier cooled respectively). The first detector for the PIXE is operated in a helium stream to measure low energy X-rays (e.g. corresponding to the K lines of low Z elements). The second one is used to analyze elements heavier than Ca and is provided with an absorber foil (e.g. 350 μm Mylar, 50 μm Al) to absorb the normally very abundant low energy X-rays, or with any mono-elemental filter whose absorption edge matches an emission line that needs selective attenuation. Gamma rays are also produced at these proton energies for the PIGE analysis [24]. They are usually detected by a large germanium detector (for example a REGe: Reverse-Electrode Ge) to determine typically: *sodium* using the 440 keV gamma rays produced by the $^{23}Na(p,p'\gamma)^{23}Na$ reaction; *lithium* using the gamma rays coming from the reactions $^{7}Li(p,n\gamma)^{7}Be$ ($E_\gamma = 429$ keV) and $^{7}Li(p,p'\gamma)^{7}Li$ ($E_\gamma = 478$ keV); *fluorine*, using the 197 keV gamma rays produced by the $^{19}F(p,p'\gamma)^{19}F$. In addition RBS analysis is performed by means of a blind surface-barrier silicon detector, under a helium flux to reduce particles energy loss, to examine samples which may have, within the proton range, a layered surface structure (e.g. a gilded metal).

A simple calculation can be made taking data from our laboratory logbook. With a 3 MeV proton beam, a current of 3.13 nA, a measure time of 240s we inject into the system 1.4×10^{13} MeV. From the target we receive X-rays, gamma, rays and backscatterd protons whose spectra, integrated in energy and time give a total "useful energy" of about 5.8×10^4 MeV for an efficiency of use of only 4.11×10^{-9}. It means that practically no energy goes into information; most of it produces in the sample a range of effects:

(1) Changes in the electronic configuration (impurities, color centers)
(2) Displacement of atoms in the sample
(3) Heating
(4) Surface sputtering
(5) Changes in composition (Implantation, new species produced by nuclear reactions)
(6) Changes in microscopic structures (formation of new phases)

The type and intensity of effects depend on the ion type, on its energy, the flux, the fluence and the target material. In absolute terms the energy and power delivered to the target are low but their effect, e.g. the power density, can be relevant when they are driven by the fluence on target which can vary of more than three orders of magnitude depending on the beam size. This is shown in Fig. 1 that resumes published data from dedicated beamlines [16–21] and, as guidelines, the calculated fluence in 1 min irradiation at a beam current of 1 nA or 100 pA. In Table 1 we calculate the power density for a 3 MeV proton high fluence beam [16,25], a 3 MeV alpha particle high fluence beam [20] and a 1.7 MeV proton low fluence beam [26], corresponding to the examples shown in Fig. 1. Power densities above 200 kW/cm^3 can be reached.

3. Passage of ions through matter

The two main mechanisms for energy loss of ions inside a material are elastic nuclear collisions and electronic excitation. Their relative importance depends on ion and energy and for a beam impinging on a sample it depends therefore on the depth of penetration into the sample up to the *projected range* i.e. its length along the input ion direction. It determines the probing depth of the IBA techniques. For a given ion the range increases with energy and can be represented by an empirical law $R = CE^\gamma$, γ being an exponent between 1 and 2 and C a constant whose value depends on the material and on the units chosen for R and E [27]. The two loss mechanisms are described by the so-called *stopping powers* or more properly *stopping forces* (either nuclear S_n or electronic S_e) that are defined as the energy loss per unit length of the trajectory [28]. Typical units for S are keV/nm. The overall dependence of the two stopping powers on energy is schematically illustrated in Fig. 2. At low energies elastic nuclear collisions provide the dominant loss mechanism, whereas the situation is the opposite for high energies. The crossing point E is not much dependent on material but rapidly increases with the mass of the bombarding ion (17 keV for B and 6 MeV for Bi). Once the energy of the ion is exhausted it stops and becomes implanted in the material.

The energy deposited by the ion may affect the structure and properties of the material mostly within the ion range, depending critically on the energy deposition mechanism and the kind of material. As a general rule the effects of the nuclear stopping power are quite independent on target material regardless of its crystallographic and electronic structure. The main effect of S_n is
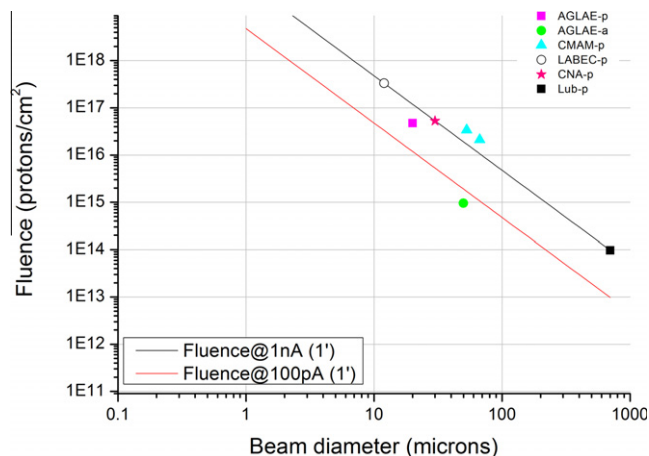
Fig. 1. The fluence as a function of the beam diameter. Points from literature are presented as well the fluence curves at 100 pA and 1 nA in 1 min.

Table 1
Range and power densities achieved in various materials in the irradiation with high and low fluence proton beams and high fluence alpha beams.

		Micro-beam		Collimated
		Protons	Alpha	Protons
	Ion Energy [MeV]	3	3	1.7
	Fluence [ions/cm^2]	5.0E+17	2.5E+15	5.0E+14
Material				
Cu	Projected range [µm]	34	5.5	14
	Power density [KW/cm^3]	234	7.3	0.32
Al	Projected range [µm]	80	11	32
	Power density [KW/cm^3]	100	3.8	0.14
CaCO$_3$	Projected range [µm]	71	9.3	28
	Power density [KW/cm^3]	112	4.3	0.16
SiO$_2$	Projected range [µm]	74	9.6	30
	Power density [KW/cm^3]	108	4.2	0.15
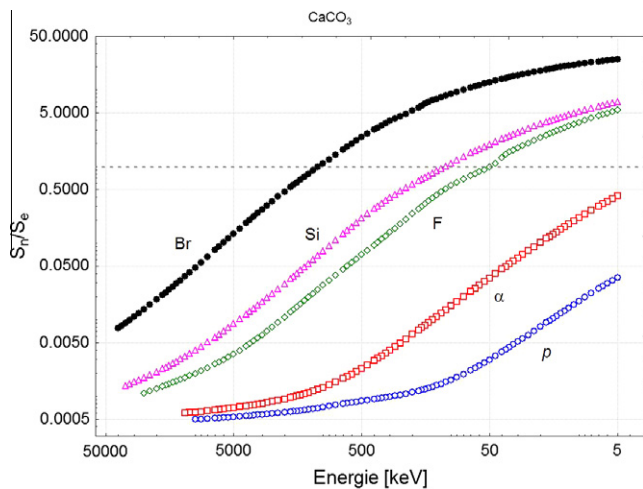
Fig. 2. The ratio between the nuclear and electronic stopping power as a function of energy calculated for some ions in CaCO$_3$.

the creation of atomic displacements and formation of Frenkel pairs (vacancies and interstitials) [29].

Other processes like nuclear reactions (inelastic scattering events) are much less important although are relevant for some applications.

The situation is completely different for the effects of the electronic energy deposition S_e. Here, the electronic structure of the material is critical. For metals, which are commonly analyzed in archaeometry, the electronic damage can be considered negligible in most cases. For the insulating materials and semiconductors the effects may be quite relevant but strongly dependent on the kind of material. Those effects do not generally produce structural damage but imply changes in the electronic distribution among the various impurities present in the material (see next section). To produce structural damage are needed ions of moderate mass ($A > 15$) and high energies (several MeV) i.e. out of the ion types and energy ranges used for archaeometry. One should also differentiate between inorganic and organic materials. Generally, inorganic materials are much more resistant to electronic excitation, whereas organic materials can be more easily damaged even at the structural level. Processes as polymerization of monomers or cross-linking of molecular chains may be readily induced by irradiation, even by light or X-rays. Even some inorganic materials, such as Cu$_3$N, are metastable and can easily decompose either thermally or under irradiation [30,31].

Although electronic damage can be of little direct relevance in many cases, electronic processes (associated to electronic excitation) may trigger side processes, such as enhanced diffusion, that may, indeed, cause relevant structural modifications.

4. Irradiation of CH objects: darkening

4.1. The darkening of the material

Since art in the past centuries has been essentially visual (not nowadays), the surface is the part of any art object that transmits to the observer the artists message. Therefore any visible change of the object, does not matter how small, is considered at first thought a serious unacceptable damage. The most visually relevant and the best studied effect of the IBA in archaeometry is indeed the darkening of the object in correspondence with the beam impact point. Some white (but not only) materials tend to darken under the action of the irradiation. Absil et al. [10] measure the gray content of the pixels of a spot image, using commercial software; Chiari et al. [11] analyze the color difference, in the CIE- Lab space, between the darkened and unchanged part of the sample; Gutierrez [32] measured the RGB coordinates of the darkened spot. Darkening increases with fluence and tends to saturate at a saturation fluence (F_{sat}) which is quite variable going from $F_{sat} = 0.6 \times 10^{13}$ p/cm^2 of Chiari et al. for a white tin lead glaze, to the $F_{sat} = 1.3 \times 10^{16}$ p/cm^2 of Absil et al. for calcium carbonate. Gutierrez does not measure saturation but gets darkening from 1×10^{15} et 2×10^{17} p/cm^2 in various materials [32]. The results of this series of analyses are summarized in Table 2. The saturation is related to the fact that two mechanisms coexist during irradiation: the creation and the destruction of color centers; therefore equilibrium is reached as the irradiation time, and consequently the charge, increase. Color centers are atomic-size structures inside a dielectric (transparent) material that absorb visible light and may present luminescence emission. In fact, luminescence is a far more sensitive (although less quantitative) tool to ascertain the presence and even identify color centers [29]. Two types of color centers are usually distinguished. The first consists of structural centers, such as vacancies and interstitials that have trapped electrons/holes and show optical transitions between energy levels. However, in most practical cases prevail color centers of the second type, i.e. transition metals or rare-earth impurities with optical transitions in the visible (or nearby) wavelength range. Each type of color center may have unpaired electrons that yield a net spin, i.e. an electron spin resonance (EPR) signal that constitutes a very reliable method to identify and characterize the center.

The stain phenomenon is to a large extent reversible [10]. The intensity of the stain shows a decrease which is a function of time and of the conditions in which the sample is kept: e.g. artificial light (room light), UV light and heat. Heating the sample will accelerate the disappearance of the stain. But it is clear that heat cannot be used freely with paintings because it would cause irreversible damage to the pigments. UV also accelerates the fading of the stains. UV light produced by a dark purple tube (used for example to detect forged notes) can alternatively make the stain disappear in less than two days without major problems, since this kind of light is commonly used by art historians to make some analyses of paintings, and should not cause any damage to the pigment. The same recovery, although with a different time constant is observed in other works [11,32].

4.2. Origin of the stain

The stain is in most cases associated to the change in the electronic charge distribution between the various impurities present in the material; this is true in particular for ancient materials, where impurities are abundant. One should remark that this effect

Table 2
A summary of established darkening conditions of some common CH materials analyzed by ion beams.

Material	Formula	Darkening	F_{sat} [p/cm^2]
Calcium carbonate	$CaCO_3$	YES	1.3×10^{16}
Lead white (cerussite)	$PbCO_3$	YES	
Pb white (hydrocerussite)	$3Pb(CO3) \cdot 2Pb(OH) \cdot 2H_2O$	YES	1.3×10^{16}
Zinc white	ZnO	YES	1×10^{15}–2×10^{17}
Titanium white	TiO_2	YES	1×10^{15}–2×10^{17}
Lead sulfate white	$PbSO_4 \cdot 3PbO \cdot H_2O$	YES	1×10^{15}–2×10^{17}
Tin Lead Yellow	Pb_2SnO or $PbSn_2 \cdot SiO_7$	NO	
Naples yellow	$Pb_3 (SbO_4)_2$	NO	
Copper Blue	$CaO \cdot CuO \cdot 4SiO_2$	NO	
Red ocre	$Fe_2O_3 \cdot nH_2$	NO	
Tin lead white glaze	SiO_2, Al_2O_3, PbO, SnO_2	YES	0.6×10^{13}
Tin lead blue glaze	SiO_2, Al_2O_3, PbO, CoO	YES	$>10^{13}$

does not necessarily involve structural changes except for the minor relaxation effects associated to the change in the local electrical charge. The primary electronic effect of ion irradiation in insulating materials is the generation of free electron–hole pairs by pumping electrons from the valence to the conduction band. In a simple approximation, that is often used, the number of pairs created per ion impact along the whole trajectory is approximately given by [33]

$$N_{e-h} \sim \frac{E}{2.5 E_G} \qquad (1)$$

E being the incoming ion energy and E_G the energy of the forbidden band gap. This means that an energy of around 2.5 E_G has to be invested per created pair (e.g. around 25–30 eV in the case of silica).The trapping of the generated charge carriers at certain impurities and/or lattice defects may induce additional absorption bands (color centers) in the transparency window of the material. Then, one can connect the area under the absorption band $OD(v)$ (the absorption coefficient at the frequency v) with the color centers areal density N through the Smakula formula [29]:

$$N = C \frac{1}{f} \frac{n}{(n^2 + 2)^2} \int OD(v) dv \qquad (2)$$

where f is the so-called oscillator strength of the corresponding optical transition ($0 < f < 1$), n the refraction index of the material and C a constant. It is, often, convenient to consider that the absorption band can be described with a Gaussian of height OD_M and width W. Then, one has the more useful expression:

$$N = 0.87 \cdot 10^{17} \frac{n}{(n^2 + 2)^2} \frac{2.303 \cdot OD_M}{d} W \qquad (3)$$

being d the thickness of the sample. The efficiency for color center creation is very dependent on the particular color center, ion energy and irradiated material. An ideal (upper efficiency limit) situation assumes that all electrons (or holes) have been trapped at a given center. According to (1) this corresponds to an energy of around 30 eV to create a color center. Therefore, irradiation with 3 MeV protons at fluences as low as 10^{11} cm^{-2} would generate a total number of 10^{16} cm^{-2} centers. Assuming a high oscillator strength ($f \approx 1$) they will cause an integrated optical density of around or above 1 that represents a quite significant absorption i.e. more than 90% of the input light beam will be absorbed. These numbers refer, indeed, to impurity centers that do not require structural modification of the material. For intrinsic color centers (such as those associated to vacancies or interstitials) the energies necessary to create a center may be much larger (maybe two orders of magnitude or more) and so appreciable darkening can only be produced at higher fluences (see next).

The situation for realistic materials may be much more complicated. Optical absorption changes have been quantified in some class of materials like the silica-based materials and the carbonates. SiO_2 is one of the compounds most extensively investigated, either as an amorphous (silica) or a crystalline phase (quartz, cristobalite,...), under different types of radiation, including X and γ rays [34–37], electrons, neutrons and ions. It constitutes the basis for a number of silicate glasses and minerals very abundant in nature and it is a majority component in large classes of human antique artefacts (glass, ceramics, jewelry). Significant studies have been performed in high purity silica or quartz (impurities at the ppm or lower level). Structural color centers, such as the E′ (silicon dangling bond), the oxygen deficient centers (ODC), and the non-bridging oxygen centers (NBOHC) are introduced by all ions in the keV and MeV energy ranges. They present absorption bands in the UV [38] and so they give no visible effects which would be compatible with studies of the historical heritage. In the CMAM we have carried out an extensive study of color center formation in SiO_2 and we have obtained that under ion bombardment (F, Cl) in the MeV range the energy needed to form one of those centers is around 10^4 eV per ion impact. At 1 MeV energy and fluences of 10^{16} cm^{-2}, one creates 10^{18} cm^{-2} centers along the projected range. Aluminum, germanium and iron impurities also may form color centers and contribute to the overall induced absorption with bands in the visible domain.

Carbonates are from a basic unit: the carbonate ion consisting of one C atom surrounded by 3 oxygen atoms in a trigonal planar arrangement. A typical carbonate material is calcium carbonate forming three main phases, calcite (hexagonal), aragonite (orthorombic) and dolomite ($CaMg(CO_3)_2$) constituting the most abundant minerals in the earth's crust. According to Table 2 calcite undergoes darkening. Electron spin resonance reveals the presence of paramagnetic defects, optical spectroscopy reveals a huge fluorescence band due to the de-excitation of F-centers [10]. Ionoluminescence (IL) combined with thermoluminescence and PIXE were used at CMAM to identify some of the recombination impurity centers introduced by irradiation. They were Mn in calcite and dolomite, Pb in cerusite and Cu in malachite and azurite [9]. These results confirm that the radiation-induced darkening is extremely sensitive to the purity of the sample and the type and concentration of contaminant impurities.

4.3. Structural studies of the irradiated material

There are a variety of analytical techniques that may provide information on the structure of the irradiated material as well as that for the color centers. They include optical techniques as Raman spectroscopy, ESR, X-ray diffraction, electron microscopy and IBA techniques. Raman spectroscopy yields information on the vibrational structure and so may serve to identify new phases or molecular species. Experiments on calcite have detected changes in the Raman spectra under PIXE radiation (protons at 2–3 MeV) [10]. On the other hand, experiments with SHI ions have

shown changes in the spectra of calcite due to the formation of CaO, associated to loss of CO_2 [39]. X-ray diffraction at grazing angle shows a small shift between the carbonates diffractive peaks in irradiated and untouched areas of the same sample. The shift is interpreted as a slight variation of the lattice parameters without the creation of new phases [32]. In any case it is very difficult for a real antique object to establish to what extent we are observing the effect of a structural damage that has changed the crystal lattice or of a redistribution of the electronic charge (electrons and holes) amongst defects and impurities already present in the object. Both effects are sure but the sensitivity of the analytical techniques (RAMAN, XRD, ESR, TL) is not sufficient to discriminate and quantify.

One should take into account that the final structure of the irradiated material results, not only, from the direct damage mechanisms but also from the side processes triggered by the synergy between irradiation, implantation and thermal effects (see next sections).

5. Irradiation of CH objects: heating

It is evident that part of the energy deposited by an ion beam in the sample goes to heat. The associated temperature increase depends on the heat capacity of the material and on the boundary conditions (sample mounting, irradiation in vacuum, etc.). In the so called "Steady State model" [40] the temperature depends on the depth of penetration of the ion in the sample, being higher at the end of range and lower at the surface. The thermal conductivity of the sample acts as a factor scale: the organic materials develop the highest temperatures reaching a few hundred degrees and the metals develop the lowest staying below 100 degrees both at fluxes of the order of $2 \cdot 10^{18}$ p/cm^2 s. The actual temperatures reached by some selected materials have been measured with the "hot probe" method [41] with protons at energies between 1.0 and 2.5 MeV, beam currents $I = 10$–100 nA, fluxes between 2×10^{11} and 2×10^{13} p/cm^2 s and fluencies between 2×10^{13} and 2×10^{15} p/cm^2. The evidence is that already at these fluencies the organic materials develop surface temperatures above 100 and up to 300 °C and that the surface may experience loss of material. In fact, those temperatures may already cause on some materials deleterious effects that should be analyzed for every particular case. In the literature several organic and delicate materials have been analyzed using IBA techniques [42–48] and we may set the safety limits of operation according to Table 3.

Inorganic materials are in principle less sensitive to temperature increases; however their analysis with high intensity microbeams requires some care because of the high power density experienced in such cases (see Table 1). There are no data available on the bulk temperature reached during the irradiation with protons and alphas as well as there have not been reports of damage due to this effect in routine IBA of CH.

Much stronger temperature increases are experienced around the ion trajectory due to the electronic energy loss, mainly in the case of heavy ions (electronic stopping regime). The temperature growth is limited to a cylinder having a cross area of a few nm diameter around the ion trajectory that gives rise to a heavily damaged region designed as *latent track* [49,50]. During irradiation there in no superposition of traces neither in space (for fluencies below 1×10^{14} - 1×10^{15} p/cm^2) nor in time (for currents below 20 nA). The structural changes caused by such thermal spike depend on the material, type of ion, and are additive with fluence [51–53].

The sequence of processes is as follows, a dense and high-energy electron–hole cloud is generated in times of the order of 10^{-16} s. In $\sim 10^{-15}$ s the energy has been redistributed among the electrons so that some effective electron temperature has been attained. Then, the electron–phonon interaction sets in and kinetic energy is being transferred to the lattice until an equilibrium temperature is reached between the electron and lattice systems after $\sim 10^{-14}$ s. The high and sudden temperature rise around the trajectory constitutes the so-called *thermal spike*, that is believed to play a key role in the structure of the damage track [54–57]. Finally, this equilibrium temperature rapidly cools down ($\sim 10^{-11}$ s) to near room temperature due to the fast heat dissipation into the virgin material. An energy balance equation can be established between the particle energy E and the kinetic E_K and potential E_P energy stored in the thermal spike. One may write, taking (1) into account and neglecting the KT term:

$$E = E_p + E_k = N_{e-h}(E_G + kT) + E_k \approx N_{e-h}E_G + E_k \approx E/2.5 + E_k \quad (4)$$

Consequently,

$$E_k \approx \frac{1.5}{2.5}E = 0.6E = gE \quad (5)$$

In other words g is the fraction of the energy deposited by the ion that goes into the temperature rise; the remaining is stored as potential energy in the e-h pairs (excitons). Once g is known the maximum temperature increment along the ion track (maintained for ultra-short time as explained above) can be estimated from the following formula [58]

$$\Delta T_{Max} = \frac{gS_e^{Max}}{\pi a_0^2 \rho C} \quad (6)$$

being ρ the density and C the specific heat of the material, S_e^{Max} the maximum of the electronic stopping force along the ion trajectory and a_0 the width of the Gaussian distribution of temperature across the ion trajectory [51]. Table 4 gives the temperature values for some materials assuming a generally accepted value $a_0 = 4$ nm. For crystalline materials ($CaCO_3$, SiO_2, SnO_2, $KAlSi_3O_8$, etc.) related with our cultural heritage and in the typical IBA conditions, i.e. with protons of 3 MeV or alphas of 12 MeV, the temperature increase should not create critical conditions such as those achieved for example in lithium niobate ($LiNbO_3$) in the electronic loss regime with higher mass ions like fluorine. In that case a complete amorphization of the material is produced in a region centered at the peak of S_e and extending progressively with the fluence (between 2×10^{14} and 1×10^{15} ions/cm^2). For CH these effects have not been studied or reported.

6. Irradiation of CH objects: enhanced atom mobility

Ion-beam irradiation may trigger a number of side processes both in the electronic as well as in the nuclear regime. One of such processes refers to the enhancement of the diffusivity of the atoms (host and impurities), particularly the lighter elements. There have been many studies reported in the literature [59,60], although the relative role of electronic and nuclear stopping has not been clarified. In the nuclear regime, binary collisions are, generally, assumed to describe the elastic ion-atom interactions and the atoms of the material are, often, considered to be on random locations. If the transferred energy T to one of the atoms overcomes a certain value E_D or *displacement energy* the knocked atom is ejected from its lattice position creating a vacancy and an interstitial, i.e. a Frenkel pair. This is the primary damage event in the nuclear regime. The primary displaced atom may in turn cause additional displacements giving rise to a heavily disordered region (displacement spike) that can alter the distribution of atoms and cause migration. The migration of light atoms, in particular sodium, has been demonstrated and quantified with low (600 keV) and high (2 MeV) protons [61–65]. With 600 keV protons there is an

Table 3
A summary of IBA operational conditions, used in the analysis of delicate organic materials in some important objects of our CH. These conditions have guaranteed the absolute safety of the procedure.

Object	Material	Energy [MeV]	Current [nA]	Diameter μm]	Flux [p/(cm²s)]	Charge [μC]	Time [s]	Fluence [p/cm²]
Historical documents	Ink Paper	1.7	1	500	3.18E + 12	1000	1000	3.18E+15
Galileo's manuscripts	Ink	2.8	0.1	200	1.99E + 12	20	200	3.98E+14
	Paper	2.8	0.05	200	9.95E+11	10	200	1.99E+14
Luca Cambiaso drawings	Ink Paper	3	0.05	60	1.11E+13	9	300	3.33E+15
Giovanni Vasari Pala Albergotti	Varnish	0.9–4.9	0.03	500	9.55E+10	12	300	2.86E+13
Antonello da Messina Ritratto Trivulzio	Varnish	0.8–5.4	0.04	500	1.27E+11	10	250	3.18E+13
Leonardo Madonna dei fusi	Varnish	2.7	0.035	1000	2.79E+10	15.4	440	1.23E+13
L. Cranach the Elder14 Nothelfer	Varnish	2.2 4	0.5	1130	3.11E+11	30	60	1.87E+13

Table 4
The maximum temperature, achievable along the ion track for some materials of interest for the CH, during irradiation with 3 MeV protons, 12 MeV alphas and 25 MeV fluorine ions. This temperature is maintained for ultra-short times.

Material	Density[g/cm²]	C[J/kgK]	ΔT(°C)H-3 MeV	ΔT(°C)He-12 MeV	ΔT(°C)F-25 MeV
$CaCO_3$	2.71	0.86	127	336	2180
H_2O	1.00	1.00	45	127	818
SiO_2	2.65	0.67–0.74	145	410	2545

enrichment of sodium in sodic or sodo-calcic glasses towards the surface at fluences of the order of 1.0×10^{17} p/cm² [61,62]. With 2 MeV protons a depletion of sodium in the region of the proton track is observed which gets more and more important with the increase of the fluence up to an 80% loss at the maximum measured fluence of 1.0×10^{17} p/cm² [64]. A microbeam (without scanning) can provide (Fig. 1) a fluence capable of mobilizing Na in an ancient glass. In the quantification of Na may exist in such cases systematic errors. One should also consider that the loss of alkali due to mobilization might cause, in the long term, mechanical damage (exfoliation). However, given the very small analysis volume and the slow speed of the exfoliation process no problems of this kind have so far been reported in archaeometry. An important point not usually considered refers to the effects of the enhanced diffusion on the degradation of the material under certain environmental conditions. As an example we may mention the rapid incorporation of atmospheric H into heavily irradiated (amorphizes) $LiNbO_3$ (CMAM, unpublished results).

7. Ion Implantation

One unavoidable effect of the application of IBA techniques is the implantation of the probing atoms. These implanted atoms modify the natural composition of the material and may induce deleterious effects such as mechanical stresses, in particular at the high fluences that may be achieved with a typical external microbeam. The implanted atoms may coalesce and form clusters, aggregates and even certain new phases. A very typical example is the formation of gas bubbles with He (and H) that may strongly weaken the mechanical resistance of the material and even lead to slicing of the upper layer. We may consider, as an example, calcium carbonate irradiated in the typical IBA conditions, i.e. with protons of 3 MeV or alphas of 12 MeV. With the SRIM [27] program we may calculate the longitudinal (r_s) and transversal (t_s) dispersion of the beam at the end of range and, knowing the beam diameter (d), the implantation volume as:

$$V_{imp} = \frac{1}{4}(d + t_s)^2 \cdot \pi \cdot r_s \quad (7)$$

The concentration of implanted ions at the fluence F will then be given by

$$[C]_{imp} = \left(F \cdot \pi \cdot \frac{d^2}{4} \right) / V_{imp} \quad (8)$$

while the concentration of atoms in the non implanted material is given by

$$[C]_{CaCO_3} = \frac{\rho N_{Avo}}{P_{Mol}} \cdot 5 \quad (9)$$

where ρ is the calcium carbonate density (2.71 g/cm³).

In Fig. 3 the beam dispersions and the implantation volume are given as a function of energy while in Fig. 4 it is given the implantation ratio. The implantation ratio at the fluence of 10^{16} particles/cm² remains below 1/1000, which is quite safe with respect to the creation of new phases; however the number of vacancies or displacements calculated by SRIM sums at $N_{disp} + N_{vac} \sim 500/\alpha$ which corresponds to ~1/2 defect/atom and at $N_{disp} + N_{vac} \sim 70/p$ which corresponds to ~1/15 defects/atom. At low energies (200 keV) the implantation ratio (around 1% with protons) and the high concentration of defects can create a heavily damaged area, appearing as a thin layer at the end of particle range, accompanied by changes in absolute volume of about 1.5%, which weaken the resistance of the target. This may be particularly relevant when irradiating the material with light elements, such as helium, that are known to form bubbles at the implanted region after suitable thermal treat-
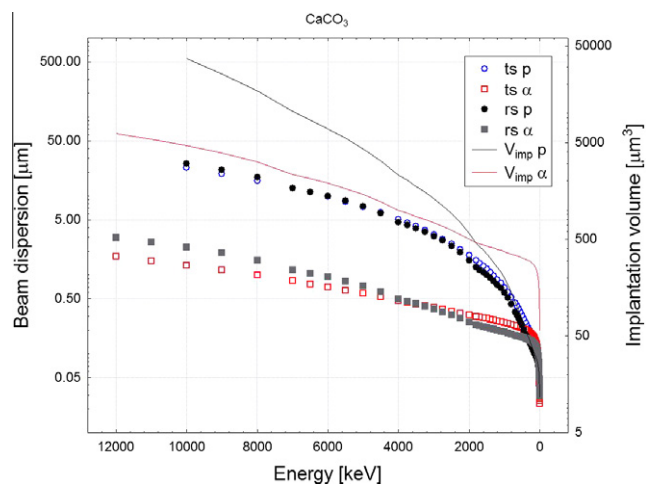
Fig. 3. The longitudinal (r_s) and transversal (t_s) dispersion as a function of energy for a beam of protons of 10 MeV maximum energy and 20 microns diameter and alphas of 12 MeV maximum energy and 50 microns diameter. The implanted volume, equation (7), is also shown. The material is $CaCO_3$.
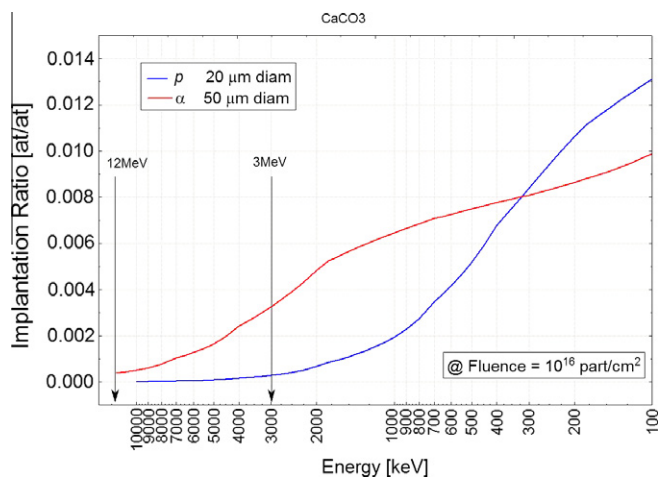
Fig. 4. The implantation ratio in atoms/atom as a function of energy for a protom beam of 20 microns diameter and an alpha beam of 50 microns diameter at a fluence of 10^{16} particles/cm^2. The material is CaCO$_3$.

Table 5
The effects of ion impact on CaCO$_3$ and gold for several ions and energies. The relative importance of ionization, holes and phonons production as well as the numer of target sputtered atoms per incoming ion are represented.

CaCO$_3$						
Ion	Energy		Primary (%)	Recoil (%)	Atoms/ ion	eV/ atom
p	3 MeV	Ionization	99.9	0.02	Ca 0	0
		Holes	0	0	C 0	0
		Phonons	0.02	0.06	O 0	0
α	12 MeV	Ionization	99.85	0.04	Ca 0	0
		Holes	0	0	C 0	0
		Phonons	0.02	0.09	O 0	0
F	25 MeV	Ionization	99.19	0.3	Ca 0	0
		Holes	0	0.02	C 0	0
		Phonons	0.03	0.47	O 0	0
Si	35 MeV	Ionization	98.83	0.49	Ca 0.016	433.54
		Holes	0	0.02	C 0	0
		Phonons	0.03	0.63	O 0.028	7.01
Br	40 MeV	Ionization	93.54	3.47	Ca 0.0846	51.72
		Holes	0.01	0.12	C 0.00769	8.68
		Phonons	0.05	2.81	O 0.1846	40.48
Au						
Br	40 MeV	Ionization	89.08	4.52		
		Holes	0.01	0.71	Au 0.8023	34.16
		Phonons	0.05	5.63		

ments. Under these conditions the weak implanted layer may allow to separate the irradiated layer from the substrate material, "Smart cutting" [66]. Structures of this kind are not expected at the energies used in archaeometry. However the volume change that accompanies a proton or alpha implantation of the kind discussed above, producing a large number of defects, could generate in principle internal pressures and micro-cracks. The process has not been studied and there is no report of short or long term visible damage of the object surface which one could correlate with the implanted layer.

8. Irradiation induced sputtering

One consequence of ion irradiation is the ejection of atoms from the surface (irradiation-induced sputtering). The effect is markedly dependent on material and irradiation conditions (ion type and energy, state of charge, target temperature, incidence angle). Also the effect is different for nuclear or electronic stopping mechanisms. In general, at the nuclear regime prevailing for light atoms the yield in ejected atoms per incident ion largely increases with ion mass.

For light ions such as H and He and MeV energies the total rate is << 1. This means that for standard fluences 10^{12}–10^{14} cm^{-2}, at most a small fraction of the upper monolayer is removed so that can be safely ignored. The effect may be enhanced when the ion and the target nucleus masses increase and might become a problem when the piece is covered by a very thin coating (nm thick). With the code SRIM a few reference values can be calculated at the extremes of the process as given in Table 5. Only for Br on Au the sputtering ratio approches 1 atom/ion. Until protons and alphas are used, metal targets can be analysed without problems. The effect may be enhanced in the electronic stopping regime when the mass of the bombarding ion is high enough. Then, the sputtering yield may reach values > 10^3 sputtered atoms/ion [67] and might become a problem when the piece is covered by a very thin coating (nm thick). Perhaps the use of heavy ion beams could be recommendable not as an analytical technique but as a very gentle and controlled way of surface cleaning competitive for example with laser cleaning [68].

9. Conclusions

The IBA techniques are used routinely in archeometry. Besides the concerted international activity and the European access programs, their success is due to the clear perception, by the final user, curator or conservator, that the integrity of the sample he is responsible of, is maintained throughout and after the analysis. The positive perception does not mean, obviously, that cultural heritage materials do not experience, like all other, the probe-target interaction and effects, but that the interaction is controllable and kept below safe limits. This work has aimed at establishing within which limits the potential damage is negligible or the analysis is viable on the basis of the benefit/cost ratio, making use of the information which is available not only from archaeometry but also from the more "aggressive" materials science applications of ion beams.

The major problem is the darkening of some materials after irradiation which seems inevitable even at the moderate fluencies necessary to a statistically significant analysis. In some cases the effect may be tolerable, in relation to the conservation status of the sample (a surface already altered by time), but the decision belongs only and exclusively to the curator. Studies of "typical" materials do not agree on the absolute amount of darkening suffered by the object but make it clear that the effect is due to the relevance of electronic damage and that it begins already at moderate fluences. The disagreement between various studies is quite certainly due to the extreme dependence on defects concentrations and therefore to the difficulty of comparing exactly the same material. We must emphasize that this type of damage can be almost completely recovered by UV annealing.

The rise in bulk temperature produced by protons and alphas at fluences typical of an archeometric IBA, is critical only in organic materials where it can reach hundreds of degrees with consequent mass losses. In archaeometry safe conditions, e.g. for the analysis of paper and paintings, have been established and well documented. With inorganic materials care should be taken only when using the high fluence microbeams; something that is normally well managed, as reported in literature. The conditions encountered in the irradiation with heavier ions (F, Si, Br) and high fluencies that lead to the amorphization of crystals (like lithium niobate), due to the accumulation of thermal spikes at the nanometer scale, are far above those applied in routine IBA of the cultural heritage and they do not constitute a problem in archaeometry.

Other potentially harmful effects are the mobilization of alkaline ion, the high concentration of defects close to the end of the ion path and surface sputtering. Under the usually conservative conditions employed in IBA of cultural heritage objects these effects are negligible; only at the high fluences possible with extracted microbeams they could produce some real damage to the

object. So far no short or long term changes have been reported in routine practice for the CH. In any case these potential effects would be limited to micrometric portions of the object, comparable with the volumes that are destroyed or sampled in SIMS, LA-ICP, TL, ICP SEM.

In conclusion the care which is usual in IBA techniques applied to our cultural heritage makes them a remarkably safe and convenient tool in terms of benefit/cost for the analysis of the precious and irreplaceable objects of our cultural heritage.

Acknowledgements

References

[1] T. Calligaro, J.C. Dran, J. Salomon, Ph. Walter, Review of accelerator gadgets for art and archaeology, Nucl. Instr. and Meth. B 226 (2004) 29–37.
[2] L. Pichon, L. Beck, Ph. Walter, B. Moignard, T. Guillou, A new mapping acquisition and processing system for simultaneous PIXE-RBS analysis with external beam, Nucl. Instr. and Meth. B 268 (2010) 2028–2033.
[3] N. Grassi, L. Giuntini, P.A. Mandò, M. Massi, Advantages of scanning-mode ion beam analysis for the study of cultural heritage, Nucl. Instr. and Meth. B 256 (2007) 712–718.
[4] J-C. Dran, J. Salomon, T. Calligaro, P. Walter, Ion beam analysis of art works: 14 years of use in the Louvre, Nucl. Instr. and Meth. B 219–220 (2004) 7–15.
[5] Ion Beam study of art and archaeological objects. A contribution by members of COST G1 action. Edited by G. Demortier, A. Adriaens, European commission, Directorate general for research, 2000, ISBN-92-828-7652-7.
[6] A. Adriaens, G. Demortier, COST Actions G1 and G8: EU programs on the use of radiation in art and archaeometry, Nucl. Instr. and Meth. B226 (2004) 3–9.
[7] Cost Action G8: Benefits of non destructive analytical techniques for conservation. Edited by A. Denker, A. Adriaens, Ch. Degrigny and J.A. Cassar, COST publication office, 2004, ISBN-92-898-0010-0.
[8] Cost Action G8: Non destructive testing and analysis of museum objects. Edited by A. Denker, A. Adriaens, M. Dowsett and A. Giumlia-Mair, Fraunhofer IRB verlag, 2006, ISBN-10:3–8167-7178-5.
[9] O. Enguita, T. Calderon, M.T. Fernandez, P. Beneitez, A. Millan, G. Garcia, Damage induced by proton irradiation in carbonate based natural painting pigments, Nucl. Instr. and Meth. B 219–220 (2004) 3–56.
[10] J. Absil, H.P. Garnir, D. Strivay, C. Oger, G. Weber, Study of color centers induced by PIXE irradiation, Nucl. Instr. & Meth. B 198 (2002) 90–97.
[11] M. Chiari, A. Migliori, P.A. Mandò, Investigation of beam-induced damage to ancient ceramics in external-PIXE measurements, Nucl. Instr. & Meth. B 188 (2002) 51–155.
[12] L. Bertrand, M.-A. Languille, S.X. Cohen, L. Robinet, C. Gervais, S. Leroy, D. Bernard, E. Le Pennec, W. Josse, J. Doucet, S. Schöder, European research platform IPANEMA at the SOLEIL synchrotron for ancient and historical materials, J. Synchrotron Rad. 18 (2011) 765–772.
[13] C. Jeynes, J. Bailey, N.J. Bright, M.E. Christopher, G.W. Grime, B.N. Jones, V.V. Palitsin, R.P. Webb, Total IBA - Where Are We?, Nucl. Instr. and Meth. In press accepted manuscript.
[14] J. Salomon, J.C. Dran, T. Guillou, B. Moignard, L. Pichon, P. Walter, F. Mathis, Present and future role of ion beam analysis in the study of cultural heritage materials: The example of the AGLAE facility, Nucl. Instr. and Meth. B 266 (2008) 2273–2278.
[15] L. Beck , L. Pichon, B. Moignard, T. Guillou, P. Walter, IBA techniques: Examples of useful combinations for the characterisation of cultural heritage materials, Nucl. Instr. and Meth. In press accepted manuscript.
[16] L. Giuntini, M. Massi, S. Calusi, The external scanning proton microprobe of Firenze: A comprehensive description, Nucl. Instr. and Meth. A 576 (2007) 266–273.
[17] O. Enguita, M.T. Fernández-Jiménez, G. Garciá, A. Climent-Font, T. Calderón, G.W. Grime, The new external microbeam facility at the 5 MV Tandetron accelerator laboratory in Madrid: beam characterisation and first results, Nucl. Instr. and Meth. B 219-220 (2004) 384–388.
[18] G. Chêne, S. Bols, T. Dupuis, A. Marchal, F. Mathis, H.-P. Garnir, D. Strivay, New external beam and particle detection set-up of Liège cyclotron - First applications of High Energy beams to Cultural Heritage, Nucl. Instr. and Meth. In press accepted manuscript.
[19] Miloš Budnar, Jure Simčič, Zdravko Rupnik, Mitja Uršiča, Primož Pelicon, Jana Kolar, Matija Strlilč, In-air PIXE set-up for automatic analysis of historical document inks, Nucl. Instr. and Meth. B 219-220 (2004) 41–47.
[20] T. Calligaro, J.-C. Dran, E. Ioannidou, B. Moignard, L. Pichon, J. Salomon, Development of an external beam nuclear microprobe on the Aglae facility of the Louvre museum, Nucl. Instr. and Meth. B 161–163 (2000) 328–333.
[21] M.Á. Ontalba Salamanca, F.J. Ager, M.D. Ynsa, B.M. Gómez Tubío, M.Á. Respaldiza, J. García López, F. Fernández-Gómez, M.L. de la Bandera, G.W. Grime, External microbeam set-up at the CNA (Sevilla) and its application to the study of Tartesic jewellery, Nucl. Instr. and Meth. B 181 (2001) 664–669.
[22] E. Ioannidou, D. Bourgarit, T. Calligaro, J.C. Dran, M. Dubus, J. Salomon, P. Walter, RBS and NRA with external beams for archaeometric applications, Nucl. Instr. and Meth. B 161–163 (2000) 730–736.
[23] T. Calligaro, J. Castaing, J.-C. Dran, B. Moignard, J.-C. Pivin, G.V.R. Prasad, J. Salomon, P. Walter, ERDA with an external helium ion micro-beam: Advantages and potential applications, Nucl. Instr. and Meth. B 1681 (2001) 180–185.
[24] A. Climent-Font, A. Muñoz-Martin, M.D. Ynsa, A. Zucchiatti, Quantification of sodium in ancient Roman glasses with ion beam analysis, Nucl. Instr. and Meth. B 266 (2008) 640–648.
[25] L.Giuntini, private communication.
[26] J. Vodopivec, M. Budnar, P. Pelicon, Application of the PIXE method to organic objects, Nucl. Instr. and Meth. B 239 (2005) 85–93.
[27] J.F. Ziegler, J.P. Biersack, M.D. Ziegler, SRIM the stopping and Range of ions in matter, Lulu Press Co, USA, 2009.
[28] E. Segre, Experimental Nuclear Physics, vol. 1, Whiley, New York, 1953.
[29] F. Agulló Lopez, C.R.A. Catlow, P.D. Townsend, Point defects in materials, Academic Press, London, 1988.
[30] R. González-Arrabal, N. Gordillo, M.S. Martín-González, R. Ruiz-Bustos, F. Agulló-López, Thermal stabilityof copper nitrate thin films:therole of the nitrogen migration, J. Appl. Phys. 107 (2010) 103513.
[31] N. Gordillo, R. González-Arrabal, A. Rivera, F. Munnik, F. Agulló-López, *Giant sputtering yields in copper nitride films Ander swift-ion irradiation: kinetics and mechanisms*, J. Phys. D (submitted 2011).
[32] P.C. Gutierrez Neira, Thesis CMAM, Univ. Autonoma Madrid, 2009, unpublished.
[33] N. Itoh, Subthreshold radiation induced processes in the bulk and on surface and interfaces of solids, Nucl. Instr. and Meth. B 135 (1998) 175–180.
[34] S.M.M. Ramos, C. Clerc, B. Canut, J. Chaumont, M. Toulemonde, H. Bernas, Damage kinetics in MeV gold ion- irradiated crystalline quartz, Nucl. Instrum. Meth. Phys. Res. B 166 (2000) 31–34.
[35] C.D. Marshall, J.A. Speth, S.A. Payne, Induced optical absorption in gamma, neutron and UV irradiated fused quartz and silica, J. Non-Crystalline Solids 59 (1997) 212.
[36] C. Davoisne, H. Leroux, M. Frère, J. Gimblot, L. Gengembre, Z. Djouadi, V. Ferreiro, L. d'Hendecourt, A. Jones, Chemical and morphological evolution of a silicate surface under low-energy ion irradiation, Astronomy and Astrophysics 482 (2008) 541–548.
[37] A.R. Bayly, Optical properties of ion bombarded silica glass, Radiation Effects 18 (1973) 11–118.
[38] S. Nagata, S. Yamamoto, A. Inouye, B. Tsuchiya, K. Toh, T. Shikama, Luminescence characteristics and defect formation in silica glasses under H and He ion irradiation, J. Nucl. Mater. 367-370 (2007) 1009–1013.
[39] S. Pabst, M. Burchard, U.A. Glasmacher, R. Miletich, R. Newmann, B. Schuster, C. Trautmann, Radiation damage in heavy ion-irradiated carbonate minerals investigated by Raman and infrared spectroscopy, GSI Scientific Report, PNI-MR-1, 2010.
[40] D.W. McColm, T.A. Cahill, The temperature profile of a microprobe, Nucl. Instr. And Meth. B 54 (1991) 91–97.
[41] D.F. Peach, D.W. Lane, M.J. Sellwood, J.D. Painter, An assessment of surface heating during ion beam analysis I: Experimental method, Nucl. Instr. and Meth. B 249 (2006) 680–683.
[42] M. Budnar, J. Simcic, M. Ursic, Z. Rupnik, P. Pelicon, Transition Metals in historic documents "Iron gall inks.on, manufacture characterization degradation and stabilization, edited by J. Kolar and M. Strlic (2006) pg. 141-146.
[43] N. Grassi, P. Bonanni, C. Mazzotta, A. Migliori, P.A. Mandò, PIXE analysis of a painting by Giorgio Vasari, X-Ray Spectrometry 38 (2009) 301–307.
[44] N. Grassi, Differential and scanning-mode external PIXE for the analysis of the painting "Ritratto Trivulzio" by Antonello da Messina, Nucl. Instr. And Meth. B 267 (2009) 825–831.
[45] C. Neelmeijer, W. Wagner, H.P. Schramm, Depth resolved ion beam analysis of objects of art, Nucl. Instr. And Meth. B 118 (1996) 338–345.
[46] F. Lucarelli, P.A. Mandò, Recent applications to the study of ancient inks with the Florence external-PIXE facility, Nucl. Instr. And Meth. B 109/110 (1996) 644–652.
[47] N. Grassi, A. Migliori, P.A. Mandò, H. Calvo del Castillo, Identification of lapis-lazuli pigments in paint layersby PIGE measurements, Nucl. Instr. And Meth. B 219-220 (2004) 48–52.
[48] A. Zucchiatti, A. Climent-Font, O. Enguita, M.T. Fernandez-Jimenez, G. Finaldi, C. Garrido, J.M. Matillas, PIXE analysis of Italian ink drawings of the XVI century, Nucl. Instr. And Meth. B 240 (2005) 520–526.
[49] N. Itoh, D.M. Duffy, S. Khakshouri, A.M. Stoneham, Making tracks: electronic excitation roles in forming swift heavy ion tracks, J. Phys.: Condens. Matter 21 (2009) 474205.
[50] M. Toulemonde, S.M.M. Ramos, H. Bernas, C. Clero, B. Canut, J. Chaumont, C. Trautmann, Mev gold irradiation induced damage in alpha-quartz: competition between nuclear and electronic stopping, Nucl. Instrum. Meth. Phys. Res. B 178 (2001) 331–336.
[51] F. Agulló-Lopez, G. Garcia, J. Olivares, Lattice preamorphization by ion irradiation: Fluence dependence of the electronic stopping power threshold for amorphization, Jour. Appl. Phys. 97 (2005) 093514.

[52] F. Agulló-López, A. Méndez, G. García, J. Olivares, J.M. Cabrera, Synergy between termal spike and exciton decay mechanisms for ion damage and amorphization by electronic excitation, Phys. Rev. B 74 (2006) 174109.

[53] J. Olivares, A. Garcia Navarro, G. Garcia, F. Agulló Lopez, F. Agulló Rueda, A. Garcia Cabanes, M. Carrascosa, Buried amorphous layers by electronic excitation in ion-beam irradiated lithium niobate: Structure and kinetics, Jour. Appl. Phys. 101 (2007) 033512.

[54] C. Dufour, A. Audouard, F. Beuneu, J. Dural, J.P. Girard, A. Hairie, M. Levalois, E. Paumier, M . Toulemonde, A high-resistivity phase induced by swift heavy-ion irradiation of Bi: a probe for thermal spike damage?, J Phys. Condensed matter 5 (1993) 4573.

[55] M. Caron, H. Rothard, M. Toulemonde, B. Gervais, M. Beuve, Theoretical and experimental study of electronic temperatures in heavy ion tracks from Auger electron spectra and thermal spike calculations, Nucl. Instr. and Meth. B 245 (2006) 36–40.

[56] Z.G. Wang, Ch. Dufour, E. Paumier, M. Toulemonde, The Se sensitivity of metals under swift-heavy-ion irradiation: a transient thermal process, J. Phys. Condens. Matter 6 (1994) 6733.

[57] Z.G. Wang, Ch. Dufour, E. Paumier, M. Toulemonde, The Se sensitivity of metals under swift heavy ions irradiation- atransient thermal process, J. Phys. Condens. Matter 7 (1995) 2525.

[58] G. Szenes, General features of latent track formation in magnetic insulators irradiated with swift heavy ions, Phys. Rev. B 51 (1995) 8026–8029.

[59] A. Ibarra, A. Muñoz-Martín, P. Martín, A. Climent-Font, E.R. Hodgson, Radiation-induced enhancement of light ions (D) in insulator materials (SiO2), J. Nucl. Mater. 367-370 (2007) 1003–1008.

[60] J.A.M. Pereira, E.F. da Silveira, Li enrichment of LiF surfaces bombarded by MeV nitrogen ion beams, Nucl. Instrum. and Meth. B 127/128 (1997) 157–159.

[61] G. Battaglin, G. Della Mea, G. De Marchi, P. Mazzoldi, A. Miotello, M. Guglielmi, Field-assisted sodium migration in glasses during medium-energy proton irradiation, J. Phys. C: Solid state 15 (1982) 5623–5627.

[62] G. Battaglin, G. Della Mea, G. De Marchi, P. Mazzoldi, A. Miotello, A. Boscolo Boscoletto, B. Tiveron, Characteristics of glass composition modification during heavy ion irradiation, Nucl. Instr. and Meth. B 19-20 (1987) 948–953.

[63] G. Arnold, G. Battaglin, G. Della Mea, G. De Marchi, P. Mazzoldi, A. Miotello, Enhanced diffusion processes during heavy ion irradiation of glasses, Nucl. Instr. and Meth. B 32 (1988) 315–317.

[64] M. Mosbah, J.P. Durand, Proton microbeam induced damage in glasses: Ca and Na distribution modification, Nucl. Instr. and Meth. B 130 (1997) 182–187.

[65] M. Mosbah, J.P. Durand, Swift proton microbeam induced diffusion in glasses, Nucl. Instr. and Meth. B 141 (1998) 594–599.

[66] Jiangang Du, Wen H. Ko, D.J. Young, Single crystal silicon MEMS fabrication based on smart-cut technique, Sensors and Actuators A112 (2004) 116–121.

[67] M. Toulemonde, W. Assmann, C. Trautmann, F. Grüner, H.D. Mieskes, H. Kucal, Z.G. Wang, Electronic sputtering of metals and insulators by swift heavy ions, Nucl. Instr. and Meth. B 212 (2003) 346–357.

[68] A. Zucchiatti, P.C. Gutiérrez Neira, A. Climent-Font, C. Escudero, M. Barrera, IBA analysis of a laser cleaned archaeological metal object: The San Esteban de Gormaz cross (Soria-Spain), Nucl. Instr. And Meth. B 269 (2011) 3115–3119.